On attenuation of seismic waves associated with flow in fractures

Data · November 2014

CITATIONS
7

READS
107

3 authors, including:

Holger Steeb
Universität Stuttgart
255 PUBLICATIONS **2,386** CITATIONS

SEE PROFILE

AGU PUBLICATIONS

Geophysical Research Letters

RESEARCH LETTER
10.1002/2014GL061634

Key Points:
- Simulate deformation-induced fluid flow in fractures and related attenuation
- Fracture flow attenuation increases with the aspect ratio of the fractures
- Simple diffusion-based models have limited approximation potential

Correspondence to:
C. Vinci,
vinci@lkm.rub.de

Citation:
Vinci, C., J. Renner, and H. Steeb (2014), On attenuation of seismic waves associated with flow in fractures, *Geophys. Res. Lett.*, *41*, doi:10.1002/2014GL061634.

Received 22 AUG 2014
Accepted 9 OCT 2014
Accepted article online 16 OCT 2014

On attenuation of seismic waves associated with flow in fractures

C. Vinci[1,2], J. Renner[2], and H. Steeb[1]

[1]Institute of Mechanics, Ruhr-Universität Bochum, Bochum, Germany, [2]Institute of Geology, Mineralogy and Geophysics, Ruhr-Universität Bochum, Bochum, Germany

Abstract Heterogeneity of porous media induces a number of fluid-flow mechanisms causing attenuation of seismic waves. Attenuation induced by squirt-type mechanisms has previously been analyzed for aspect ratios smaller or equal to 10^3. Using a hybrid-dimensional modeling approach, particularly apt for large aspect ratio conduits, we numerically simulated deformation-induced fluid flow along two intersecting fractures to investigate the physics of attenuation related to the interaction of fracture-induced fluid flow and to leak-off. Attenuation related to fracture flow increases in magnitude with increasing geometrical aspect ratio of the fracture. The inherent time scales of both flow mechanisms do not influence each other, but the faster process is associated with stronger attenuation than the slower process. Models relying on simple diffusion equations have rather limited potential for approximation of pressure transients.

1. Introduction

Elastic waves propagating in fluid-saturated rocks are attenuated by a number of mechanisms. *Biot* [1956] described the fluid flow on the wavelength scale induced by deformation of homogeneous poroelastic media. Flow mechanisms, not captured by this continuum approach, are related to the specific geometrical characteristics of the pore space or to the presence of cracks [*Li et al.*, 2001; *Mavko et al.*, 2009]. Inhomogeneous distributions of rock matrix properties and hydraulic properties induce heterogeneous effective stresses and fluid pressure distributions, causing fluid flow on the length scale of the heterogeneities. In a fractured material, fluid flow may occur in a single conduit or between conduits when the material volume is stressed [*Rubino et al.*, 2013, 2014].

Real rocks comprise voids of vastly different geometry. Often, the term *pore* is reserved for close to isometric voids on grain scale. The term *fracture* is used to address a second prototype of void that typically has one dimension falling significantly short of the other two. Their long dimension can vary from grain scale to way beyond it.

The term *squirt flow* [*Mavko and Nur*, 1979; *Dvorkin and Nur*, 1993; *Chapman et al.*, 2002; *Adelinet et al.*, 2011] denotes flow of a viscous fluid at the microstructure scale. Pressure diffusion and resulting energy loss induced by squirt-type mechanisms have been previously analyzed for conduit geometries characterized by a length-aperture ratio (aspect ratio) smaller or equal to 10^3 [*Rubino et al.*, 2013, 2014; *Quintal et al.*, 2014]. Yet natural or stimulated fractures in reservoirs exhibit high aspect ratios and resemble thin and elongated inclusions with aspect ratios $> 10^3$ [e.g., *Seeburger and Zoback*, 1982; *Olson*, 2003]. Here the term *fracture flow* is used to address energy loss, i.e., viscous dissipation, related to fluid flow in conduits with large aspect ratios causing attenuation of waves.

In the following, we numerically investigate fluid flow induced by elastic deformation of fractures that are much larger than the average pore size of a porous rock. We employ a two-dimensional prototype cell comprising two fractures intersecting each other at a normal angle hosted in a homogeneous porous matrix. The numerical implementation allows us to independently study the effects of flow within a fracture, between fractures, and between fractures and porous matrix. The dissipative flow mechanisms lead to time dependence of the deformation. The different mechanisms are actually associated with characteristic times varying with the properties of pores and fractures. We quantify the observed deformation evolution by the frequency dependence of inverse quality factors, i.e., measures for attenuation. An improved understanding of the role of attenuation due to flow in fractures with realistic aspect ratios provides new directions for the

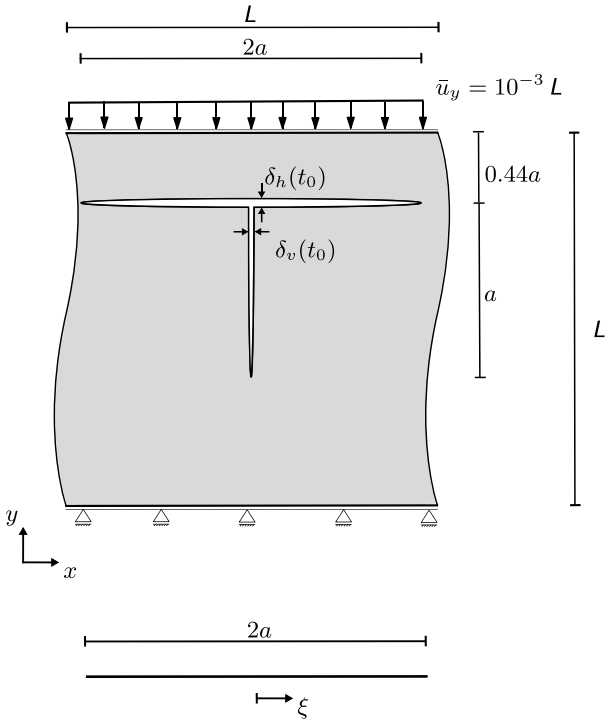

Figure 1. Geometry of the two-dimensional unit cell: (top) poroelastic rock containing two interconnected fractures. The horizontal and vertical fractures have a maximum aperture at time $t_0 = 0$ s equal to $\delta_h(t_0)$ and $\delta_v(t_0)$, respectively. Displacement $\bar{u}_y$ is imposed on the top edge. The bottom edge is constrained with respect to vertical displacement and is undrained ($q = 0$). At the left and right edges, periodic boundary conditions are applied with respect to both horizontal displacements and fluid flux. (bottom) One-dimensional domain of the horizontal fracture as employed in the flow problem.

interpretation of field data, for example, estimation of fracture parameters from seismic data [e.g., *Bakulin et al.*, 2000] or analysis of fracture connectivity [e.g., *Berkowitz et al.*, 2000; *Rubino et al.*, 2013; *Quintal et al.*, 2014].

2. Modeling Approach

A simple two-dimensional unit cell is analyzed that consists of a poroelastic rock sample with two intersecting elliptical fractures (Figure 1). Even though a two-dimensional cell is an obvious simplification of real rocks, the unit cell contains the relevant end-member features responsible for contrasting physical processes. The horizontal fracture acts as a fluid-storage domain, and its deformation triggers fluid exchange with and therefore the flow in the vertical (or arbitrarily oriented) fracture. Either fracture may exchange fluid with the poroelastic matrix along their entire surfaces.

The porous rock matrix and the fractures are saturated with a compressible, viscous pore fluid (dynamic viscosity $\eta^{f,R}$ and compressibility $\beta_f = 1/K^f$, Table 1). Extending previous investigations [e.g., *Rubino and Holliger*, 2013; *Rubino et al.*, 2013], the hydro-mechanical phenomena are investigated for high aspect ratio features, i.e., the apertures δ_v and δ_h of the vertical and horizontal fractures are much smaller than their lengths, $\delta_h, \delta_v \ll a$ (Figure 1, top). The half length $a = 5$ cm applies for both fractures and is approximately 2 orders of magnitude larger than the typical length scale of pores in reservoir rocks [e.g., *Dullien*, 1991]. The unit cell size is $L = 2.2\,a$. The horizontal and vertical fractures are modeled as an ellipse and as a half ellipse, respectively. The vertical fracture intersects the horizontal one at its center.

Uniaxial compression is imposed by a vertical displacement boundary condition $\bar{u}_y = 10^{-3}\,L$ applied at the top edge of the unit cell, enforced linearly in a time span $t_{appl} = 10^{-8}$ s, which we choose as the sampling

Table 1. Material Parameters Applied in the Numerical Investigations[a]

Fractures in Unit Cell	Surrounding Rock	
$L = 2.2\,a$	$K^s = 36$ GPa	grain
$a = 5$ cm	$K_d = 16$ GPa	skeleton
$\delta_h(t_0) = 100$ μm	$G = 16$ GPa	skeleton
	$D = 2.6 \times 10^{-5}\ \frac{m^2}{s}$	for $k^s = 10^{-18}$ m^2
	$K^f = 2.3$ GPa	fluid
	$\eta^{f,R} = 0.001$ Pa s	fluid
	$\phi = 0.01$	
$\delta_v(t_0) = 10$ μm	$k^s = 10^{-30}$ m^2	case (a)
$\delta_v(t_0) = 10$ μm (undeformable)	$k^s = 10^{-18}$ m^2	case (b)
$\delta_v(t_0) = 10$ μm	$k^s = 10^{-18}$ m^2	case (c)
$\delta_v(t_0) = 5$ to 500 μm	$k^s = 10^{-30}$ m^2	parameter study

[a] $D = \frac{k^s}{\eta^{f,R} s}$; $s = \frac{1}{K_d} + \frac{\phi}{K^f} - \frac{1+\phi}{K^s} = 3.88 \times 10^{-11}$ Pa^{-1}

interval in the postprocessing. An individual simulation covers 10^{16} samples leading to a frequency range from 10^{-8} Hz to 10^{8} Hz that allows for a comprehensive analysis of the frequency dependence of attenuation. Vertical displacements are prohibited for the lower edge, and no-flux boundary conditions are applied on the top and bottom edges. Furthermore, periodic boundary conditions are used for the pore pressure and the solid displacements on the left and right edges [*Jänicke et al.*, 2015].

Through hydro-mechanical coupling, the deformation-induced pressure gradients trigger fluid exchange between fracture domains and rock matrix, here addressed as leak-off independent of actual flow direction and controlled by the hydraulic diffusivity of the matrix. The vertical compression of the horizontal fracture induces fluid flow into the vertical one. Fluid flow along the fractures is affected by the fracture transmissivity as well as by deformation of the fracture through hydro-mechanical coupling effects [*Vinci et al.*, 2014].

2.1. Governing Equations

2.1.1. Hydro-mechanical Approach

Following *Quintal et al.* [2011], we investigate wave-induced fluid flow and the hydro-mechanical coupling in the matrix domain of the unit cell by solving Biot's quasi-static poroelastic equations [e.g., *Biot*, 1941; *Detournay and Cheng*, 1995]. To solve the time-dependent set of poroelastic equations numerically, the quasi-static finite element method is used in a displacement-pressure formulation [e.g., *Zienkiewicz et al.*, 1999; *Quintal et al.*, 2011]. Since this investigation focuses on fractured poroelastic domains, the poroelastic modeling framework is extended by the previously presented hybrid-dimensional approach [*Vinci et al.*, 2014] allowing for an efficient numerical solution of hydro-mechanical problems of fluid-filled fractures with aspect ratios $> 10^3$. The fluid flow in the deformable fractures is accounted for by a one-dimensional approach leading to the governing equation

$$\frac{\partial p}{\partial t} + \frac{1}{12\eta^{\mathrm{fR}}}\frac{\partial}{\partial \xi}\left(-\frac{\delta_i^2}{\beta_{\mathrm{f}}}\frac{\partial p}{\partial \xi}\right) - \left(\frac{\delta_i}{12\eta^{\mathrm{fR}}\beta_{\mathrm{f}}}\frac{\partial \delta_i}{\partial \xi}\right)\frac{\partial p}{\partial \xi} - \frac{\delta_i^2}{12\eta^{\mathrm{fR}}}\left(\frac{\partial p}{\partial \xi}\right)^2 = -\frac{1}{\beta_{\mathrm{f}}\delta_i}\frac{\partial \delta_i}{\partial t} + q_L, \tag{1}$$

where δ_i, with $i = h, v$, represents the apertures of the horizontal and the vertical fractures with local coordinate ξ (Figure 1). The modeling equation (1) comprises, in order from left to right, a transient term, a diffusion term, a nozzle (convection) term, a quadratic term, and a hydro-mechanical coupling term. The source term q_L accounts for leak-off. In the performed simulations, the magnitude of the applied boundary condition at the top edge is chosen small, and therefore, the influence of the quadratic, i.e., nonlinear, term remains negligible and is not further discussed (see dimensional analysis in *Vinci et al.* [2014]). The variations in apertures $\delta_i(\xi, t)$, which affect the local transmissivity (permeability) of the fracture $T_F(\xi) = \delta_i^3/12$ as well as the quadratic term, are evaluated together with the fluid pressure $p(\xi, t)$ with the theory of poroelasticity [*Biot*, 1941] and equation (1), respectively, and are used as coupling variables between the one-dimensional fracture flow process and the two-dimensional poroelastic problem.

In each discrete time step of the numerical simulations, total and effective stresses, fluid pressure, displacements, and seepage velocities are calculated inside the unit cell. Following the methodology described in *Quintal et al.* [2011], volume-averaged stresses and strains are calculated in a postprocessing step. The complex effective stiffness of the unit cell $M(f) = \bar{\sigma}_{yy}/\bar{\varepsilon}_{s,yy}$ relates Fourier-transformed averages of total stress $\bar{\sigma}_{yy}(f)$ and strain $\bar{\varepsilon}_{s,yy}(f)$ of the unit cell [see also *Pride and Masson*, 2006]. The inverse quality factor $Q^{-1} := \mathrm{Im}(M)/\mathrm{Re}(M)$ is evaluated to describe the characteristics of the dissipative effects in a compact way. The frequency dependence of $M(f)$ (and Q) allows us to analyze characteristic frequencies f_c (inverse characteristic relaxation times), i.e., frequencies where the inverse quality factor Q^{-1} peaks. The complex effective stiffness $M(f)$ affects the velocity and attenuation of longitudinal and shear waves.

2.1.2. Diffusion-Based Approach

Simple diffusion models have previously been used to approximate the characteristics of flow in fractures [e.g., *Cooper et al.*, 1967; *van Everdingen and Meyer*, 1971; *Gringarten et al.*, 1974]. For the analyzed unit cell, fracture flow mainly occurs in the vertical fracture; therefore, we present a diffusion-based approach that models the flow in the vertical fracture only. The simple diffusion equation governing fluid flow along the vertical fracture reads

$$\frac{S_F}{\bar{\delta}_v}\frac{\partial p}{\partial t} - \frac{\bar{\delta}_v^2}{12\eta^{\mathrm{fR}}}\frac{\partial^2 p}{\partial \xi^2} = 0, \tag{2}$$

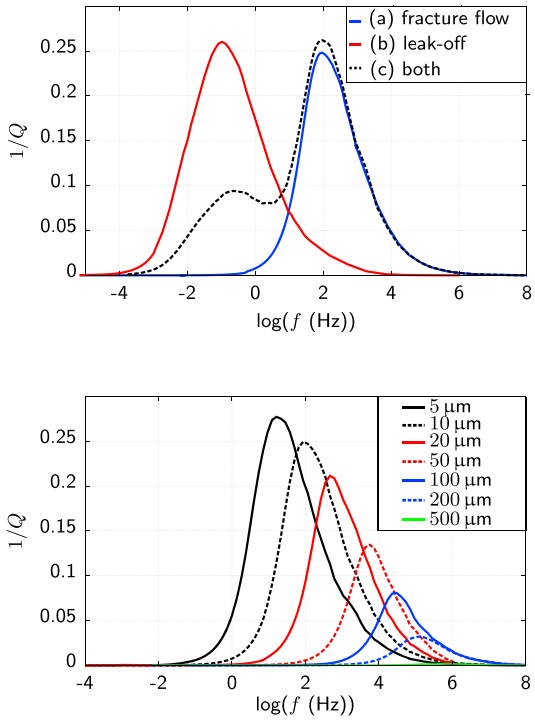

Figure 2. (top) Inverse quality factor for (a) fracture flow only (blue line, $k^s = 10^{-30}$ m^2), (b) leak-off only (red line, $k^s = 10^{-18}$ m^2, undeformable fractures), and (c) for both processes (black dashed line); (bottom) effect of initial vertical fracture aperture $\delta_v(t_0)$ at $t_0 = 0$ s (as indicated by label) on the inverse quality factor $1/Q$ for fracture flow only.

[e.g., *Mavko et al.*, 2009] introducing the mean aperture $\bar{\delta}_v$. Storage capacity S_F and transmissibility $T_F = \bar{\delta}_v^3/12$ are accounted for as single macroscopic properties though pressure is calculated locally. For deformable fractures, the bulk storage capacity

$$S_F = S_F^d = \bar{\delta}_v \beta_f + \frac{\partial \bar{\delta}_v}{\partial p} \tag{3}$$

has two contributions [*Ortiz et al.*, 2011, 2013], one deriving from the fluid compressibility β_f and one from changes in the mean fracture aperture $\bar{\delta}_v$ caused by pressure variations. Here we neglect details of the fracture deformation and express its contribution to the storage capacity by parameterization of the bulk storage capacity in multiples of the fluid compressibility, i.e.,

$$S_F = \alpha_s S_F^r \approx \alpha_s \delta_{v0}(t_0) \beta_f, \tag{4}$$

where S_F^r denotes the bulk storage capacity of a rigid fracture and $\delta_{v0}(t_0)$, the maximum fracture aperture at time $t_0 = 0$ s, approximates the mean aperture of the vertical fracture $\bar{\delta}_v(t_0)$ with deviations within approximately 20%.

2.2. Sets of Simulations

Exploratory numerical calculations employed a vertical fracture with an initial aperture $\delta_v(t_0) = 10$ μm corresponding to an aspect ratio $2a/\delta_v = 10^4$. Three cases were investigated: (a) fracture flow in an impermeable elastic rock, (b) leak-off between undeformable fractures and permeable poroelastic rocks, and (c) fracture flow coupled with leak-off from deformable fractures in poroelastic rocks. In case (a), an impermeable rock is modeled by assigning an artificially low intrinsic permeability $k^s = 10^{-30}$ m^2 to the matrix material (Table 1). In case (b), undeformable fractures, i.e., with $\bar{\delta}_v(t) = \text{const}$ and, therefore, $\partial \bar{\delta}_v/\partial t = 0$, are analyzed that are embedded in a permeable rock with permeability $k^s = 10^{-18}$ m^2, dry bulk modulus $K_d = 16$ GPa, and mineral's average modulus $K^s = 36$ GPa. The chosen permeability value and bulk moduli are representative for crystalline basement rocks [e.g., *Brace*, 1980; *Gebrande*, 1982; *Ingebritsen and Manning*, 1999].

In a second set of numerical simulations, we investigated the effect of the aperture of the vertical fracture on attenuation. We neglected leak-off (as in case (a); see Table 1) to concentrate on the physics of attenuation caused by fracture flow.

In a third set of numerical investigations, we analyzed to which extent terms in equation (1) other than diffusion affect the attenuation characteristics. In addition to results obtained for the hydro-mechanically coupled model, approaches are analyzed that reduce the vertical fracture to a nondeformable conduit while maintaining compliance for the horizontal fracture, the storage feature (fluid source) in our model. Furthermore, effects related to the nozzling (convection) term are quantified comparing numerical results of a model that accounts for convection with those of a model where convection effects are suppressed. The nozzling term is proportional to the pressure gradient and to the aperture gradient and is eliminated when modeling the vertical fracture with a rectangular shape. In this case, the flow process in the vertical fracture is approximated with a simple diffusion equation.

3. Results

For an impermeable matrix, a single attenuation process occurs (pure fracture flow). The associated inverse quality factor exhibits a single maximum at a characteristic frequency $f_{c,ff} \sim 10^2$ Hz for

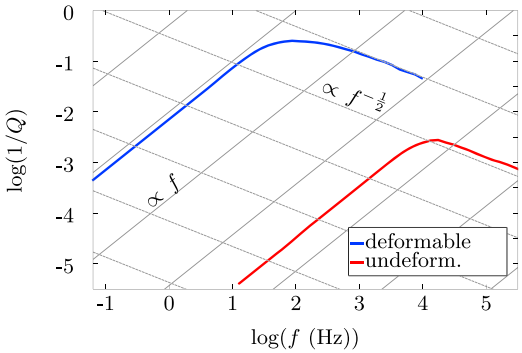

Figure 3. Inverse quality factor for a deformable (blue line) and an undeformable (red line) vertical fracture of initial aperture $\delta_v(t_0) = 10$ μm. An impermeable rock matrix is approximated by $k^s = 10^{-30}$ m^2. Both distribution functions of $1/Q$ exhibit the identical scaling behavior in agreement with classical power law relations [e.g., *Mueller et al.*, 2010].

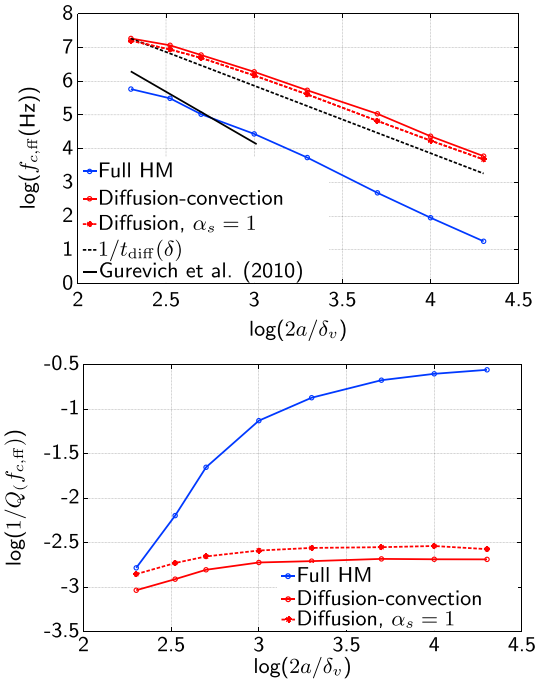

Figure 4. (top) Characteristic frequencies as varying with aspect ratio (impermeable matrix) for the full hydro-mechanical coupled problem (blue line), neglecting coupling effects (red line), and assuming simple diffusion, i.e., with $\alpha_s = 1$ (red dashed line). Characteristic frequencies from simple diffusion time (black dashed line) and estimated characteristic frequencies of fracture flow proposed by *Rubino and Holliger* [2013] and *Gurevich et al.* [2010] (black line). (bottom) Comparison of full hydro-mechanical results, diffusion and convection, and simple diffusion: amplitude of log(1/*Q*) at the characteristic frequency $f_{c,ff}$ versus dimensionless parameter $\log(2a/\delta_v)$.

an aspect ratio of 2×10^4 (Figure 2, top). In case of undeformable fractures, only the rock matrix deforms, and leak-off constitutes the only attenuation process giving rise to a single peak in $1/Q$ at a frequency $f_{c,lo} \sim 10^{-1}$ Hz (Figure 2, top). The absolute values of the peaks of the inverse quality factor are comparable for fracture flow and leak-off. For a permeable matrix comprising deformable fractures, both fracture flow and leak-off occur. The inverse quality factor exhibits two peaks at the characteristic frequencies $f_{c,ff} \sim 10^2$ Hz and $f_{c,lo} \sim 10^{-1}$ Hz (Figure 2, top).

3.1. Effect of Aspect Ratio of the Vertical Fracture on Attenuation

For some combinations of geometrical parameters, fracture stiffness, and rock permeability, attenuation due to fracture flow is quantitatively similar or stronger than dissipation due to leak-off (Figure 2, bottom). An increase of the aspect ratio of the vertical fracture from 2×10^2 to 2×10^4 causes an increase of the magnitude of attenuation related to fracture flow by approximately 1 order of magnitude. Furthermore, the lower the initial aperture $\delta_v(t_0)$ is, the lower the characteristic frequency $f_{c,ff}$. For high aspect ratio fractures, attenuation induced by fracture flow is observed at frequencies typical for seismic surveys ($f < 10^2$ Hz).

3.2. Effect of Fracture Deformation on Attenuation

Comparing a simulation for an undeformable fracture to one including hydro-mechanical coupling shows that the flow process along the undeformable fracture is characterized by a shorter characteristic time (higher characteristic frequency, Figure 3). For the chosen geometry and material properties (Table 1, case (a)), the characteristic frequency of fluid flow in an undeformable fracture is approximately 2 orders of magnitude higher than the one for a deformable fracture. The peak height shows the opposite behavior; deformable fractures cause attenuation that exceeds the one associated with undeformable fractures by 2 orders of magnitude (Figure 3). Both distribution functions of $1/Q$ exhibit the identical scaling behavior (despite different processes) in agreement with classical power law relations [e.g., *Mueller et al.*, 2010].

3.3. Effect of Convection and Hydro-mechanical Coupling on Characteristic Frequencies and Magnitude of Attenuation

Modeling fracture flow with a simple diffusion equation yields characteristic frequencies $f_{c,\mathrm{diff}}$ and magnitudes of the inverse quality factor differing by various orders of magnitude from those obtained by employing the hybrid-dimensional approach (Figures 3 and 4). Specifically, the difference in maximum of $1/Q$ between the hydro-mechanical solutions and the diffusion-based solutions diminishes with increasing initial aperture $\delta_v(t_0)$ (Figure 4, bottom).

Neglecting hydro-mechanical coupling in the simulations shifts the characteristic frequencies toward the frequency values representative of a simple diffusion model governed by equation (2). The nozzling term is responsible for a slight increase in characteristic frequency compared to a simple transient diffusion process, i.e., $\alpha_s = 1$ in equation (4).

Increasing the storage multiplier α_s in equation (4) can account for fracture deformation in a simplified way. With adequate values of α_s, one can either match the characteristic frequency or the maximum in $1/Q$ obtained with a simple diffusion equation to the ones resulting from a fully hydro-mechanically coupled model. For example, the characteristic frequencies were matched choosing $\alpha_s = 10^1$ to 10^4 following an approximate power law relation with δ_v of $\alpha_s \approx \delta_v^{-1.1}\, c_1$, where c_1 depends on the chosen geometry and material parameters. This relation, however, does not simultaneously lead to a match for the maximum in inverse quality factor.

4. Discussion

We investigated interconnected fractures that exchange fluid mass by fluid flow in them (here termed *fracture flow*) upon their deformation. When the two fractures do not intersect, the interfracture flow mechanism does not take place and attenuation is only related to flow within an individual fracture that is negligible compared to attenuation due to interfracture flow or leak-off effects, a finding previously presented by *Rubino et al.* [2013] that we confirmed relying on our approach. We refrain from reporting our calculations that exceed the current scope.

4.1. Characterization of Fluid Flow Mechanisms

An inversely proportional relation was proposed between the characteristic frequency of squirt flow and the cube of the aspect ratio of cracks [*Mavko et al.*, 2009; *Pride et al.*, 2003]; in qualitative agreement, our calculations yield $f_{c,\mathrm{ff}} \propto (2a/\delta_v)^{-2.3}$ and reasonable quantitative agreement to the squirt-flow relation of *Gurevich et al.* [2010] in the range of overlapping frequencies despite the difference in exponent (Figure 4, top). Criticism was raised that within the squirt-flow concept, unrealistic aspect ratios have to be invoked to explain observed peaks in the inverse quality factor in the range of frequencies covered by various types of measurements [*Pride et al.*, 2004]. When associated with flow on grain scale, i.e., from compressed to extended grain boundary fractures, for example, the range of characteristic frequencies is limited because the range of realistic aspect ratios is limited. When typical grain sizes of 100 μm to 1 mm determine fracture length, unrealistic fracture widths below 0.1 μm result for aspect ratios exceeding 10^3 for the inverse cubic relation. The lower exponent of our relation somewhat reduces this problem. Yet typical mesoscopic features with lengths various orders of magnitude larger than grain size [e.g., *Olson*, 2003; *Neuman*, 2008] still exhibit realistic widths in the range of hundreds of micrometer to millimeter for aspect ratios of 10^4 and larger. As shown by our calculations, the characteristic frequency related to flow in fractures with aspect ratios larger than 10^3 can explain attenuation occurring in the range of geophysical exploration methods relying on elastic waves (Figure 4, top).

The fluid transport processes between the fractures and the matrix are distinctly transient; therefore, the controlling parameter for flow in the matrix is its diffusivity, comprising permeability, and specific storage capacity. In the present investigation we did not vary the matrix's storage capacity but only its permeability. In our poroelastic formulation, specific storage capacity of the matrix is controlled by the choice of the drained modulus for the matrix, a parameter we kept constant throughout the modeling. Therefore, the characteristic frequency $f_{c,\mathrm{lo}}$ apparently depends only on permeability of the surrounding rock (compare also *Rubino et al.*, 2013) within the framework of our numerical investigation while in reality any microstructural change causing an alteration of permeability will likely also affect storage properties [e.g., *Song and Renner*, 2008], and thus, diffusivity rather than permeability has to be considered.

For leak-off, the higher the permeability of the surrounding rock is, the faster the process. The observed characteristic frequency $f_{c,lo} \sim 10^{-1}$ Hz (Figure 2, top) is fairly well approximated employing the scaling relation for diffusion $f_{c,diff} \sim L_{diff}^2/D$ when approximating the characteristic length of the diffusion problem by the mean distance between matrix material and drained surfaces, $L_{diff} \sim 0.5\,a$ and using the diffusivity D (Table 1) [*Zimmerman et al.*, 1986; *Kuempel*, 1991].

The characteristic frequency $f_{c,ff}$ depends strongly on the aperture of the fracture, the larger the aperture the larger the permeability and therefore the faster the flow process. In the overlapping range of aspect ratios, characteristic frequencies of the fully coupled model lie near the frequencies presented by *Rubino and Holliger* [2013] and *Gurevich et al.* [2010] (Figure 4, top). The investigation of *Rubino and Holliger* [2013] corresponds to the high-frequency end of our investigation, where resolution problems are encountered related to the chosen time step that affect the entire distribution of 1/Q. The analytical fit provided by *Gurevich et al.* [2010] of their numerical results exhibits a slightly different slope than our numerical results for higher aspect ratios, corresponding to a misfit in characteristic frequency of about 1 order of magnitude at an aspect ratio of 10^4.

Owing to the hydro-mechanical coupling effects on fluid transport, the characteristic frequency for fracture flow $f_{c,ff}$ corresponds to a characteristic time that cannot, in general, be estimated from the scaling relation for a simple diffusion process [*Chapman et al.*, 2003]. For a rigid fracture filled with a compressible fluid, the characteristic diffusion time results to

$$t_{c,diff} \sim \frac{(2a)^2}{D_F}, \tag{5}$$

where $D_F = T_F/S_F^r\eta^{fR}$. The considered geometries yield short times of $t_{c,diff} \approx 10^{-7}$ to 10^{-3} s, values that correspond to characteristic frequencies several orders of magnitude larger than frequencies obtained with the hydro-mechanical model (Figure 4, top). Deformability of the fracture decreases the characteristic frequency considerably for given aspect ratio, i.e., the contributions from the physical processes covered by the governing equation (1) beyond diffusion are significant.

The maximum value of $1/Q$ for undeformable fractures is various orders of magnitude lower than the one associated with fluid flow through deformable fractures. The extent of attenuation is controlled by the storage capacity of the fractures. A lower mass exchange between the horizontal and the vertical fractures—owing to the smaller storage capacity of the vertical fracture—results in less attenuation. Differences in attenuation between the hydro-mechanical problem and the undeformable-fracture solution depend on the aspect ratio $2a/\delta_v$ of the vertical fracture (Figure 4, bottom). Deviations are large for high aspect ratios and diminish with decreasing aspect ratio.

One may account for the deformability of the fracture by parameterization of its specific storage capacity as in equation (4). The found power law relation between the optimized α_s values for matching characteristic frequencies exhibits close qualitative and quantitative resemblance to $\alpha_s = c_{static}\delta^{-1}$ with $c_{static} = 4\,a\,K^f(3K_d+4G)/G(12K_d+4G) \sim 0.0126$ m, found when simplistically using the relation between width and uniform pressure for ellipsoidal fractures [e.g, *Valkó and Economides*, 1995] to approximate $\partial\bar{\delta}_v/\partial p$ in equation (3). This order-of-magnitude approximation can guide to use diffusion models as approximations of hydro-mechanically coupled problems.

4.2. Interaction Between Fluid Flow Mechanisms

In the presented unit cell, comprising fractures with $2a/\delta_v = 10^4$, the characteristic frequencies $f_{c,ff}$ and $f_{c,lo}$, at which the inverse quality factor reaches maxima, remain unaltered when fracture flow and leak-off operate simultaneously (Figure 2, top). Apparently, the two processes do not influence each other with respect to characteristic time scales. On the contrary, the maximum in the inverse quality factor for leak-off is affected by the presence of fracture flow.

For the investigated cases of deformable fractures, an intrinsic permeability of the rock $k^s = 10^{-18}$ m^2 is large enough to allow for leak-off to take place and small enough to avoid an overlap of the two characteristic attenuation phenomena (Figure 2, top). For deformable fractures in a permeable matrix, fracture flow only takes place when its characteristic time scale is smaller than that for leak-off. Then, pressure gradients in the fractures are first equilibrated by flow in them before leak-off equilibrates fractures and matrix. In contrast, if $f_{c,lo} \gg f_{c,ff}$, i.e., in case of a highly permeable rock matrix, all pressure inhomogeneities, both,

between the fracture domains and the matrix and within the matrix, are dissipated by fluid flow in the matrix. Pressure gradients are already dissipated on the scale of the characteristic time of fracture flow, and thus, fluid flow along the fractures is negligible.

5. Conclusions

Attenuation effects, i.e., loss of deformation energy, were investigated in a two-dimensional unit cell containing two interconnected fractures intersecting at a normal angle embedded in a homogeneous poroelastic matrix. The attenuation effects were related to fracture flow in the vertical fracture and fluid exchange between the fractures and the surrounding rock (leak-off). Fracture flow was induced by deformation of the horizontal fracture, triggering fluid mass exchange between the horizontal and the vertical fracture. Using a hybrid-dimensional approach, particularly apt for high aspect ratio fractures, fluid flow in the fractures was modeled as a one-dimensional process, while the fluid flow at the pore scale was described by the theory of poroelasticity. Leak-off and fracture flow are related to distinct characteristic frequencies that do not influence each other. In contrast, the magnitude of attenuation for leak-off and fracture flow is affected by coupled processes. The faster process, i.e., the one with the higher characteristic frequency, dissipates the pressure gradients in the unit cell before the slower process can become active. Thus, the faster process is characterized by stronger attenuation than the slower process.

The contribution of fracture flow to attenuation in the seismic frequency range increases in magnitude with increasing aspect ratio of inclusions. To correctly account for fracture flow, hydro-mechanical coupling effects have to be considered. Restricting to diffusion phenomena cannot capture the full characteristics of attenuation in fractured poroelastic media. Neglecting hydro-mechanical coupling results in attenuation related to fracture flow orders of magnitude smaller than for results obtained with a hydro-mechanically coupled model. The quantitative discrepancy increases with increasing aspect ratio of the vertical fracture.

Acknowledgments

We thank Ralf Jänicke for providing the MATLAB scripts to evaluate the inverse quality factor. Simulation results and data used to generate figures are available upon request via e-mail to the first author. We thank the benevolent assessment of an anonymous reviewer and the in-depth comments of Beatriz Quintal.

Andrew Newman thanks two anonymous reviewers for their assistance in evaluating this paper.

References

Adelinet, M., J. Fortin, and Y. Guégen (2011), Dispersion of elastic moduli in a porous-cracked rock: Theoretical predictions for squirt-flow, *Tectonophysics*, *503*(1–2), 173–181.

Bakulin, A., V. Grechka, and I. Tsvankin (2000), Estimation of fracture parameters from reflection seismic data: Part I: HTI model due to a single fracture set, *Geophysics*, *65*(6), 1788–1802.

Berkowitz, B., O. Bour, P. Davy, and N. Odling (2000), Scaling of fracture connectivity in geological formations, *Geophys. Res. Lett.*, *27*(14), 2061–2064.

Biot, M. A. (1941), General theory of three-dimensional consolidation, *J. Appl. Phys.*, *12*, 155–164.

Biot, M. A. (1956), Theory of propagation of elastic waves in a fluid-saturated porous solid. I. Low-frequency range, *J. Acoust. Soc. Am.*, *28*, 168–178.

Brace, W. (1980), Permeability of crystalline and argillaceous rocks, *Int. J. Rock Mech. Min. Sci. Geomech. Abstr.*, *17*(5), 241–251.

Chapman, M., S. V. Zatsepin, and S. Crampin (2002), Derivation of a microstructural poroelastic model, *Geophys. J. Int.*, *151*, 427–451.

Chapman, M., S. Maultzsch, and E. Liu (2003), Estimating the squirt-flow frequency, paper presented at 65th EAGE Conference and Exhibition - Session Rock Physics - Theory, Stavanger, Norway, 2-5 June.

Cooper, H., Jr., J. Bredehoeft, and I. Papadopulos (1967), Response of a finite-diameter well to an instantaneous charge of water, *Water Resour. Res.*, *3*, 263–269.

Detournay, E., and A.-D. Cheng (1995), Fundamentals of poroelasticity, in *Comprehensive Rock Engineering: Principles, Practice and Projects*, edited by C. Fairhurst, p. 752, Pergamon, Oxford, U. K.

Dullien, F. A. (1991), *Porous Media: Fluid Transport and Pore Structure*, 574 pp., Academic, Waltham, Mass.

Dvorkin, J., and A. Nur (1993), Dynamic poroelasticity: A unified model with the squirt and the Biot mechanisms, *Geophysics*, *58*(4), 524–533.

Gebrande, H. (1982), Elastic wave velocities and constants of rocks and rock forming minerals, in *Landolt-Börnstein*, vol. 1b, edited by G. Angenheister, pp. 1–34, Springer, Berlin.

Gringarten, A., H. J. Ramey, and R. Raghavan (1974), Unsteady-state pressure distributions created by a well with a single infinite-conductivity vertical fracture, *Soc. Pet. Eng. J.*, *14*, 347–360.

Gurevich, B., D. Makarynska, O. Bastos de Paula, and M. Pervukhina (2010), A simple model for squirt-flow dispersion and attenuation in fluid-saturated granular rocks, *Geophysics*, *75*, 109–120.

Ingebritsen, S., and C. Manning (1999), Geological implications of a permeability-depth curve for the continental crust, *Geology*, *27*, 1107–1110.

Jänicke, R., B. Quintal, and H. Steeb (2015), Numerical homogenization of mesoscopic loss in poroelastic media, *Eur. J. Mech. A. Solids*, *49*, 382–395, doi:10.1016/j.euromechsol.2014.08.011.

Kuempel, H. (1991), Poroelasticity: Parameters reviewed, *Geophys. J. Int.*, *105*, 783–799.

Li, X., L. Zhong, and L. Pyrak-Nolte (2001), Physics of partially saturated porous media: Residual saturation and seismic-wave propagation, *Annu. Rev. Earth Planet. Sci.*, *29*, 419–460.

Mavko, G., and A. Nur (1979), Wave attenuation in partially saturated rocks, *Geophysics*, *44*, 161–178.

Mavko, G., T. Mukerji, and J. Dvorkin (2009), *The Rock Physics Handbook: Tools for Seismic Analysis of Porous Media*, 542 pp., Cambridge Univ. Press, Cambridge, U. K.

Mueller, T., B. Gurevich, and M. Lebedev (2010), Seismic wave attenuation and dispersion resulting from wave-induced flow in porous rocks a review, *Geophysics*, *75*, 147–164.

Neuman, S. (2008), Multiscale relationships between fracture length, aperture, density and permeability, *Geophys. Res. Lett.*, *35*, L22402, doi:10.1029/2008GL035622.
Olson, J. E. (2003), Sublinear scaling of fracture aperture versus length: An exception or the rule?, *J. Geophys. Res.*, *108*(B9), 2413, doi:10.1029/2001JB000419.
Ortiz, A., R. Jung, and J. Renner (2013), Two-dimensional numerical investigations on the termination of bilinear flow in fractures, *J. Geophys. Res. Solid Earth*, *4*, 331–345, doi:10.5194/se-4-331-2013.
Ortiz, A. E., J. Renner, and R. Jung (2011), Hydro-mechanical analyses of the hydraulic stimulation of borehole Basel 1, *Geophys. J. Int.*, *185*, 1266–1287.
Pride, S., and Y. Masson (2006), Acoustic attenuation in self-affine porous structures, *Phys. Rev. Lett.*, *97*, 184,301.
Pride, S. R., et al. (2003), Permeability dependence of seismic amplitudes, *Leading Edge*, *22*, 518–525.
Pride, S. R., J. G. Berryman, and J. M. Harris (2004), Seismic attenuation due to wave-induced flow, *J. Geophys. Res.*, *109*, B01201, doi:10.1029/2003JB002639.
Quintal, B., H. Steeb, M. Frehner, and S. Schmalholz (2011), Quasi-static finite element modeling of seismic attenuation and dispersion due to wave-induced fluid flow in poroelastic media, *J. Geophys. Res.*, *116*, B01201, doi:10.1029/2010JB007475.
Quintal, B., R. Jänicke, J. Rubino, H. Steeb, and K. Holliger (2014), Sensitivity of S-wave attenuation to the connectivity of fractures in fluid-saturated rocks, *Geophysics*, *79*, WB15–WB24.
Rubino, J. G., and K. Holliger (2013), Research note: Seismic attenuation due to wave-induced fluid flow, *Geophys. Prospect.*, *61*, 882–889.
Rubino, J. G., L. Guarracino, T. Müller, and K. Holliger (2013), Do seismic waves sense fracture connectivity?, *Geophys. Res. Lett.*, *40*, 692–696, doi:10.1002/grl.50127.
Rubino, J. G., T. Müller, L. Guarracino, M. Milani, and K. Holliger (2014), Seismoacoustic signatures of fracture connectivity, *J. Geophys. Res. Solid Earth*, *119*, 2252–2271, doi:10.1002/2013JB010567.
Seeburger, D., and M. Zoback (1982), The distribution of natural fractures and joints at depth in crystalline rock, *J. Geophys. Res.*, *87*, 5517–5534.
Song, I., and J. Renner (2008), Hydro-mechanical properties of Fontainebleau sandstone: Experimental determination and micromechanical modeling, *J. Geophys. Res.*, *113*, B09211, doi:10.1029/2007JB005055.
Valkó, P., and M. Economides (1995), *Hydraulic Fracture Mechanics*, 318 pp., John Wiley, Hoboken, N. J.
van Everdingen, A., and L. Meyer (1971), Analysis of buildup curves obtained after well treatment, *Soc. Pet. Eng. J.*, *23*(4), 513–524.
Vinci, C., J. Renner, and H. Steeb (2014), A hybrid-dimensional approach for an efficient numerical modeling of the hydro-mechanics of fractures, *Water Resour. Res.*, *50*, 1616–1635, doi:10.1002/2013WR014154.
Zienkiewicz, O. C., A. Chan, M. Pastor, B. Schrefler, and T. Shiomin (1999), *Computational Geomechanics With Special Reference to Earthquake Engineering*, John Wiley, Hoboken, N. J.
Zimmerman, R., W. Somerton, and M. King (1986), Compressibility of porous rocks, *J. Geophys. Res.*, *91*, 12,765–12,777.